Nanoscale Horizons

ROYAL SOCIETY OF CHEMISTRY

COMMUNICATION

View Article Online
View Journal

Cite this: DOI: 10.1039/d5nh00206k

Received 4th April 2025,
Accepted 4th June 2025

DOI: 10.1039/d5nh00206k

rsc.li/nanoscale-horizons

Pinocytosis inhibitory nanoparticles enhance aPD-1 antibody delivery and efficacy while avoiding toxicity in the treatment of solid tumors†

Stephanie R. Zelenetz,‡[ab] Haeik Park,‡[ab] Wenan Qiang,[bcd] Gan Lin,[abe] Sultan Almunif,[abf] Swagat H. Sharma,[ab] Debora B. Scariot,[abe] Junlin Lu,[bg] Robert W. Reichert,[ab] Bin Zhang[dh] and Evan A. Scott *[abe]

While monoclonal antibodies have significantly improved cancer treatment, their accumulation in off-target tissues not only limits efficacy, but also induces toxicity. A major contributor to this problem is the mononuclear phagocyte system (MPS). This collection of innate immune cells is a critical regulator of immune homeostasis that effectively scavenges nanoparticles and biologics, preventing their therapeutic effects within solid tumors. Here, pinocytosis inhibitory nanoparticles are demonstrated to safely and temporarily disable the MPS *via* enhanced delivery of the small molecule actin inhibitor latrunculin A (LatA). This "indirect targeting" strategy is applied to improve anti-programmed death receptor 1 (aPD-1) antibody administration in mice bearing melanoma and colon carcinoma, decreasing aPD-1 interaction with the MPS, avoiding liver toxicity, increasing engagement with target cells, and modulating the immune microenvironment of solid tumors. The resulting change in biodistribution significantly improved safety, anticancer efficacy, and overall survival. Our methodology may be employed to enhance a wide range of monoclonal antibody therapies.

New concepts

Monoclonal antibodies have emerged as an important modality in cancer treatment, boasting superior specificity to chemotherapy and radiation. However, suboptimal biodistribution and unwanted clearance can limit therapeutic antibody efficacy and safety. A major contributor to this is the mononuclear phagocyte system (MPS), a collection of innate immune cells that passively sample the environment around them to maintain homeostasis *via* a process called pinocytosis, and unfortunately as a result, also scavenge therapeutics. In this work, we employ a strategy called "indirect targeting" using pinocytosis inhibitory nanoparticles to safely and temporarily disable antibody uptake by the MPS, a problem that has largely been overlooked in antibody delivery. This approach was used to ameliorate the biodistribution of the monoclonal antibody anti-programmed death receptor-1 (aPD-1) by decreasing its accumulation in off-target tissues and promoting its engagement with target cells in solid tumors. This enhanced delivery translated to significant improvements in both the efficacy and safety of aPD-1 treatment. Additionally, this strategy does not rely on antigen or tissue-specific features and avoids the need to modify antibody structure or administration, making it a broadly applicable drug delivery strategy.

While cancer remains a leading cause of death worldwide, advancements in diagnosis and treatment continue to increase survival rates.[1] In particular, the development and application of new monoclonal antibody targets and therapeutic strategies in the clinic have yielded remarkable progress.[2] The bioactivity of these drugs is typically more selective than small molecule chemotherapeutics, which can reduce off-target effects.[3] However, poor biodistribution and rapid systemic clearance can prevent antibodies from reaching their targets within safe and tolerable ranges of dosage, hindering the usage of new

[a] Department of Biomedical Engineering, Northwestern University, Evanston 60208, Illinois, USA. E-mail: evan.scott@northwestern.edu
[b] Chemistry of Life Processes Institute, Northwestern University, Evanston 60208, Illinois, USA
[c] Department of Obstetrics and Gynecology, Department of Pathology, Feinberg School of Medicine, Northwestern University, Chicago 60611, Illinois, USA
[d] Robert H. Lurie Comprehensive Cancer Center of Northwestern University, Chicago 60611, Illinois, USA
[e] Department of Biomedical Engineering, NanoSTAR Institute, University of Virginia School of Medicine, Charlottesville 22908, Virginia, USA
[f] Bioengineering Institute, King Abdulaziz City for Science and Technology, Riydah 12354, Saudi Arabia
[g] Department of Chemical and Biological Engineering, Northwestern University, Evanston 60208, Illinois, USA
[h] Department of Medicine, Hematology/Oncology Division, Feinberg School of Medicine, Northwestern University, Chicago 60611, Illinois, USA

† Electronic supplementary information (ESI) available: ^{1}H NMR spectrum and GPC data of synthesized polymer (Fig. S1); DLS, physiochemical properties and encapsulation efficiency of LatA-PS (Fig. S2) LatA viability on RAW 264.7 macrophages by flow cytometry (Fig. S3); *in vitro* uptake of DiD-PS after LatA-PS incubation in DC2.4 cells (Fig. S4); IVIS image of mice showing aPD-1 tumor uptake over 2 days (Fig. S5); representative flow cytometry plots of aPD-1 accumulation on a cellular level (Fig. S6); PhenoCycler images of myeloid cells in the TME with increased saturation (Fig. S7); PhenoCycler images of myeloid cells in the TME (Fig. S8); tumor images, Ki67 staining, body weight measurements and heart histology of mice (Fig. S9). See DOI: https://doi.org/10.1039/d5nh00206k

‡ S. R. Z. and H. P. contributed equally to this work.

pharmaceutical constructs employing antibodies like antibody–drug conjugates (ADCs) and radiotherapies.[4,5]

Many factors hinder the delivery of therapeutic antibodies. After systemic injection, antibodies exit the vasculature and enter tissues primarily through convection. This process is limited by the large size and hydrophilicity of monoclonal antibodies, and only 5–15 percent of the administered therapeutic distributes from the blood to tissues.[6,7] In the context of cancer, barriers in the tumor microenvironment (TME) further hinder antibody delivery. Aberrant vasculature, resulting in poor blood flow and vascular permeability, can reduce transport to the site of the tumor. The high hydrostatic pressure and dense extracellular matrix in the TME can physically prevent antibody penetration. Additionally, once at the site of the tumor, the antibody's activity can be hindered by changes in antigen expression, including mutation and downregulation, which limit the ability of the drug to engage with its target. Finally, clearance at the tumor, which occurs *via* proteolysis after cellular internalization, can further dampen efficacy.[8,9]

The mononuclear phagocyte system (MPS) consists of a broad range of phagocytic cell populations, including macrophages, monocytes and dendritic cells that are spread throughout the body. These cells are important regulators of immune homeostasis and critical modulators of drug delivery and clearance. While passively sampling their surroundings to alert for signs of foreign compounds and danger, they can uptake therapeutics *via* pinocytosis, limiting target interactions and efficacy.[10,11] Organs containing concentrated populations of MPS cells overlap with sites of drug off-target accumulation and toxicity, notably the liver, lung, kidney and spleen.[12] For many pharmaceuticals, including antibody-based therapeutics, the MPS has been proven to have a significant impact on biodistribution and clearance.[11,13] Thus, the MPS is an additional—and critical—modulator of therapeutic antibody efficacy and safety, and an important consideration in drug delivery.

Evan A. Scott

Nanoscale Horizons provides a critical and much needed outlet for new concepts in nanotechnology and was instrumental in the success of our research. Our first Nanoscale Horizons manuscript was a review article that we published back in 2019 to promote an underutilized yet highly promising nanostructure, the bicontinuous nanosphere. This spearheaded our work with this nanoparticle, leading to multiple subsequent publications and funded grant proposals. We again went to Nanoscale Horizons in 2021 to present our proof-of-concept data for our "indirect targeting" strategy, which we are honored to build upon here in our contribution to their well-earned 10th anniversary collection.

Previous work to improve antibody delivery has consisted of both active and passive targeting strategies. For example, protein- and glyco-engineering approaches to increase neonatal Fc receptor (FcRn) binding have been shown to prevent antibody catabolism after cellular internalization.[14] Other attempts have included modifying the isoelectric point of the antibody and increasing affinity for the target antigen, though the latter has not been shown to impact clearance. Changing the amino acid sequence of the antibody can also cause unwanted immunogenicity.[14,15] For ADCs and radiotherapies, bioorthogonal chemistry is under investigation for targeting tumor-specific receptors.[16] In aggregate, these attempts represent efforts to prevent drug clearance and increase half-life, which is correlated with therapeutic efficacy.[17] Unfortunately, such strategies largely fail to acknowledge the MPS, and a need exists for an orthogonal and broadly applicable method of directly avoiding accumulation of antibody therapeutics within MPS cells and organs.

In this work, we propose employing the strategy of "indirect targeting" to ameliorate therapeutic antibody biodistribution by inhibiting off-target accumulation within the MPS (Scheme 1).[18,19] Antibody internalization is prevented *via* the targeted administration of latrunculin A (LatA), a small molecule actin inhibitor that hinders pinocytosis. Our group has previously demonstrated that the pre-administration of LatA-loaded nanoparticles enhances the accumulation of subsequently injected cancer cell-targeted nanoparticles in solid tumors by minimizing their MPS clearance in the liver, spleen, and lymph nodes.[18] Here, we investigate this method to improve the delivery and therapeutic efficacy of anti-programmed death receptor-1 (aPD-1), an immune checkpoint inhibitor (ICI) monoclonal antibody that has been employed for the treatment of over 15 different types of cancer.[20] Initial validation of enhanced solid tumor targeting was performed using B16F10 melanomas. We then assessed therapeutic efficacy in CT26 murine carcinomas, a well-characterized solid tumor model frequently employed to investigate changes in anticancer immunity and tumor growth due to its highly inflamed TME and responsiveness to aPD-1 treatment.[21] Since LatA is hydrophobic and has poor water solubility, we encapsulated it within nanoparticles consisting of poly(ethylene glycol)-*b*-poly(propylene sulfide) (PEG-*b*-PPS), a non-toxic, self-assembling block copolymer with validated utility in drug delivery.[18,22,23] Moreover, nanoparticles consisting of PEG-*b*-PPS are a strong choice for targeting the MPS. The PEG corona of these nanoparticles prevents nonspecific uptake, allowing for selective targeting of phagocytic cells without the need for active targeting strategies.[24,25] Additionally, the oxidation sensitivity of the block-copolymer promotes nanoparticle disassembly in the lysosome, facilitating intracellular cargo release and the formation of polymer chains small enough to be rapidly cleared by the kidney.[26] Nanostructure morphology was optimized for MPS targeting, and polymersomes, rather than micelles, were chosen for this work due to their higher systemic stability and accumulation within cells of the MPS.[27]

In this proof-of concept work, we found that indirect targeting can limit aPD-1 uptake by the MPS and increase its interaction

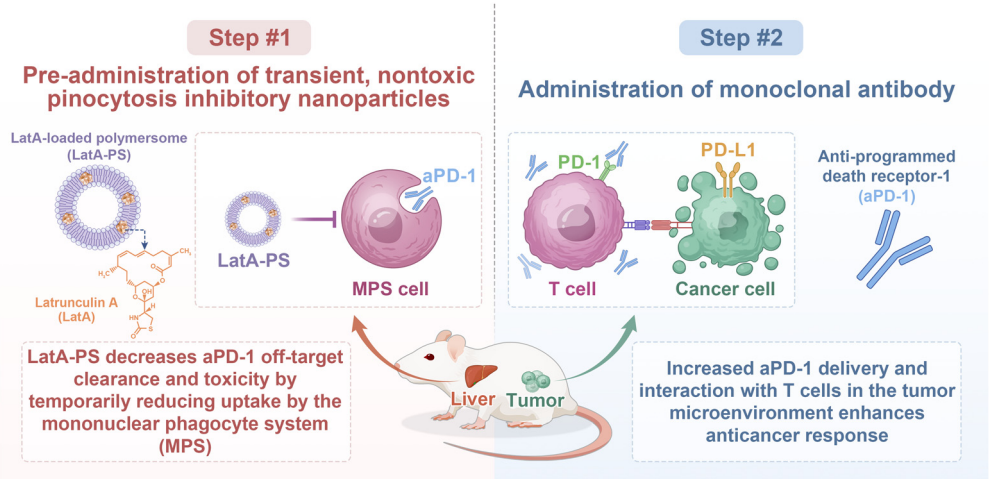

Scheme 1 Overview of the "indirect targeting" strategy for improving monoclonal antibody accumulation and efficacy in solid tumors *via* priming with latrunculin-A-loaded polymersome (LatA-PS) injections.

with T cells. Importantly, we show that LatA can generate significant enhancements in the anticancer efficacy, while meaningfully reducing the systemic toxicity, generated by aPD-1.[28,29] Both *in vitro* and *in vivo* results show encapsulation within nanocarriers was necessary to avoid toxicity of free form LatA. Given it is antigen- and tissue-agonistic and that our pre-injection protocol avoids the need to modify the formulation or administration of the monoclonal antibody, we believe these pinocytosis inhibitory nanoparticles can improve the delivery of a wide variety of therapeutic antibodies across tumor-type and disease indication to have a significant clinical impact.

Results and discussion

Characterization of LatA-PS

LatA-loaded polymersomes (LatA-PS) were formed from the self-assembly of methoxy poly(ethylene glycol)-*b*-poly(propylene sulfide)-benzyl ($mPEG_{17}$-PPS_{30}-Bz) *via* thin film hydration as previously described.[23] Polymer purity was confirmed with ^1H nuclear magnetic resonance (NMR) spectroscopy and gel permeation chromatography (GPC) (Fig. S1, ESI†). Cryogenic-transmission election microscopy (cryo-TEM) and small angle X-ray scattering (SAXS) confirmed the vesicular nanoparticle morphology (Fig. 1A and B). Dynamic light scattering was used to determine the *z*-average, polydispersity and zeta potential of LatA-PS, which were 97.0 nm, 0.24, and −3.8 mV respectively (Fig. S2, ESI†). Particle diameter and membrane thickness were also determined by SAXS, which were estimated to be 65.0 nm, and 9.5 nm, respectively (Fig. S2B, ESI†). LatA loaded well within the nanoparticles, with an encapsulation efficiency of 45.8 percent, as determined by reverse-phase high performance liquid chromatography (RP-HPLC, Fig. S2B, ESI†).

LatA-PS are potent actin inhibitors *in vitro*

In vitro studies were performed to determine the cellular effects of LatA and LatA-PS. Since LatA, an inhibitor of actin polymerization, is known to be cytotoxic at high concentrations, viability studies were completed.[30] For this, an MTT assay was performed on both RAW 264.7 macrophages (Fig. 1C) and CT26 cells (Fig. 1D), which were incubated with free LatA or LatA-PS for 24 h. Flow cytometry was also performed to assess viability on RAW 264.7 macrophages (Fig. S3, ESI†). Untreated cells were used as a control. The effect of LatA on cell viability was concentration dependent. Additionally, polymersome encapsulation significantly reduced LatA toxicity, consistent with past findings regarding LatA-micelle encapsulation.[18]

After showing polymersome encapsulation mitigates LatA's known cytotoxicity, the ability of LatA-PS to affect actin polymerization was investigated. RAW 264.7 macrophages were incubated with either LatA-PS or PBS, stained with NucBlue™ and Alexa-Fluour™ 488-Phalloidin, a dye that binds actin filaments (F-actin), and imaged with confocal microscopy (Fig. 1E).[31] Untreated cells displayed expansive actin networks throughout the cell, while those treated with LatA-PS had less F-actin present, indicating interference with actin polymerization. Additionally, cells incubated with LatA-PS had a rounded, rather than spindle-like, morphology, further suggesting that LatA affected the actin cytoskeleton.[31,32]

LatA has been previously shown to decrease nanoparticle uptake by inhibiting macropinocytosis, which occurs in as little as 30 min and maintains peak efficacy for greater than one hour after drug removal (Fig. S4, ESI†). However, its influence on antibody uptake; which can occur through multiple receptor-dependent and independent pathways including antigen-binding, Fc receptor (FcR) binding and pinocytosis; had yet to be determined.[18,33] To investigate this, RAW 264.7 macrophages were treated, or primed, with LatA-PS or PBS for 24 h and then incubated with Flamma® Fluors 648-labeled-aPD-1 for 2 h. Remaining aPD-1 in solution was washed away, and the amount of aPD-1 engaged with cells was determined by fluorescence (Fig. 1F). Cells treated with LatA-PS were found to have significantly less aPD-1 interaction, decreasing mean fluorescent intensity (MFI) by up to 4.3-fold. Inhibition of cellular uptake was confirmed by confocal microscopy. RAW 264.7 cells were primed

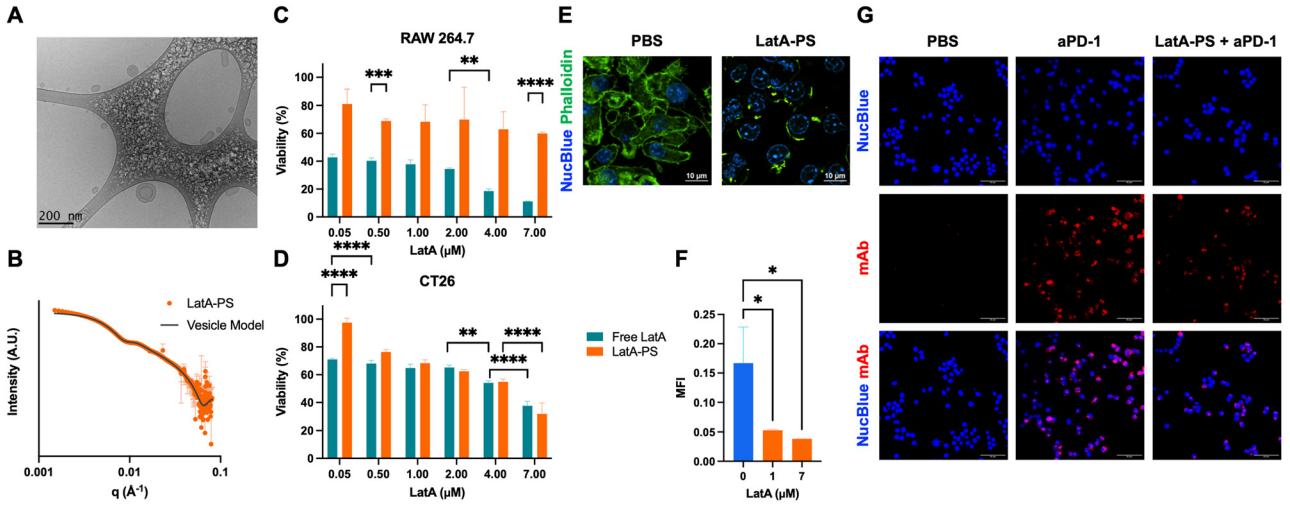

Fig. 1 Material characterization and effects of latrunculin A-loaded polymersomes (LatA-PS) *in vitro*. Vesicular polymersome morphology for LatA-PS was verified by (A) cryogenic transmission electron microscopy (n = 3) and (B) small angle X-ray scattering (SAXS, n = 2). Cytotoxicity and cell proliferation of (C) RAW 264.7 macrophages and (D) CT26 cells after 24 h in culture with free LatA or LatA-PS was assessed using an MTT assay (n = 3). (E) RAW 264.7 macrophages treated with LatA-PS for 24 h and then stained with NucBlue™ and AlexaFluour™ 488-Phalloidin were imaged with confocal microscopy (n = 3) scale bar represents 10 μm. (F) Mean fluorescence intensity (MFI) of RAW 264.7 macrophages treated with LatA-PS for 24 h and then Flamma® Fluors 648-labeled-aPD-1 for 2 h (n = 3). (G) Representative confocal microscopy of RAW 264.7 macrophages treated with LatA for 30 min and then incubated with Flamma® Fluors 648-labeled aPD-1 for 15 min demonstrated decreased aPD-1 uptake (n = 3 technical replicates, n = 1 biological replicate). Scale bar represents 50 μm. All data are reported as mean ± sd, * p-value < 0.05, ** p-value < 0.01, *** p-value < 0.001, **** p-value < 0.001 (ANOVA).

with LatA for 30 min, treated with Flamma® Fluors 648-labeled-aPD-1 for 15 min, and stained with NucBlue™. Confocal revealed a lower number of cells positive for aPD-1 upon treatment with LatA-PS (Fig. 1G). Collectively, these results demonstrate that LatA can block the cellular internalization of aPD-1 by relevant cells within the MPS.

LatA-PS priming facilitates indirect targeting of tumors *in vivo*

To determine if LatA-PS priming could promote indirect targeting of tumors, enhancing therapeutic antibody accumulation in tumor tissue and reducing uptake in MPS organs, mice bearing melanoma were treated with free LatA or LatA-PS and Flamma® Fluors 648-labeled-aPD-1 (Fig. 2). Briefly, C57BL/6 mice were injected subcutaneously with 5×10^5 B16F10 cells and tumors were allowed to grow to 100 mm^3. Mice received two 7 μM injections of either free LatA or LatA-PS at 24 h and 4 h prior to aPD-1 administration, according to an established dosing regimen.[18] Mice then received a single 100 μg injection of Flamma® Fluors 648-labeled-aPD-1. Untreated mice and mice receiving only aPD-1 were used as controls. An *in vivo* imaging system (IVIS) was employed to measure aPD-1 uptake, with the imaging angle optimized to visualize aPD-1 tumor accumulation in real time. At 2 days-post aPD-1 injection, mice were sacrificed and aPD-1 uptake in the heart, lung, spleen, liver, kidney and tumor, were assessed *ex vivo* (Fig. 2A). Total radiant efficiency was calculated for each organ using the Living Image™ software.

IVIS imaging showed LatA priming to significantly increase aPD-1 accumulation in the tumor over the course of 2 days post-injection (Fig. 2B, C and Fig. S5, ESI†). That is, pre-administration of free LatA or LatA-PS increased the aPD-1 signal 7-fold and 5.4-fold, compared to aPD-1 injection alone, respectively (Fig. 2C). This increase in tumor accumulation might be attributed at least in part to decreased MPS uptake, which can promote antibody clearance, and may have allowed more aPD-1 to circulate and reach target tissues.[11,13] Altogether, these results suggest that LatA priming allows for the indirect targeting of tumors, by promoting accumulation in the TME.

LatA-PS priming promotes indirect targeting of aPD-1 on a cellular-level

We anticipated that the shift in organ-level biodistribution of aPD-1 would be accompanied by changes at the cellular level. To test this, mice bearing colon carcinoma were treated with Flamma® Fluors 648-labeled-aPD-1 in the presence or absence of free LatA or LatA-PS (Fig. 3). A CT26, rather than B16F10, model was selected for cellular-level antibody biodistribution, immunomodulation and tumor growth inhibition experiments due to the CT26 model's increased immune infiltration and PD-L1 expression in the TME, which confer better responsiveness to ICIs.[34,35] Additionally, since we only sought to change the biodistribution of the therapeutic antibody, rather than its mechanism of action, choosing a model already well-established to respond to aPD-1 treatment was paramount. Briefly, mice were injected subcutaneously with 2×10^5 CT26 cells and began treatment when tumor volumes reached approximately 120 mm^3. Mice receiving treatment were administered 10 mg kg^{-1} aPD-1 three times, once every 3 days. Mice primed with LatA received either 7 μM free LatA or LatA-PS

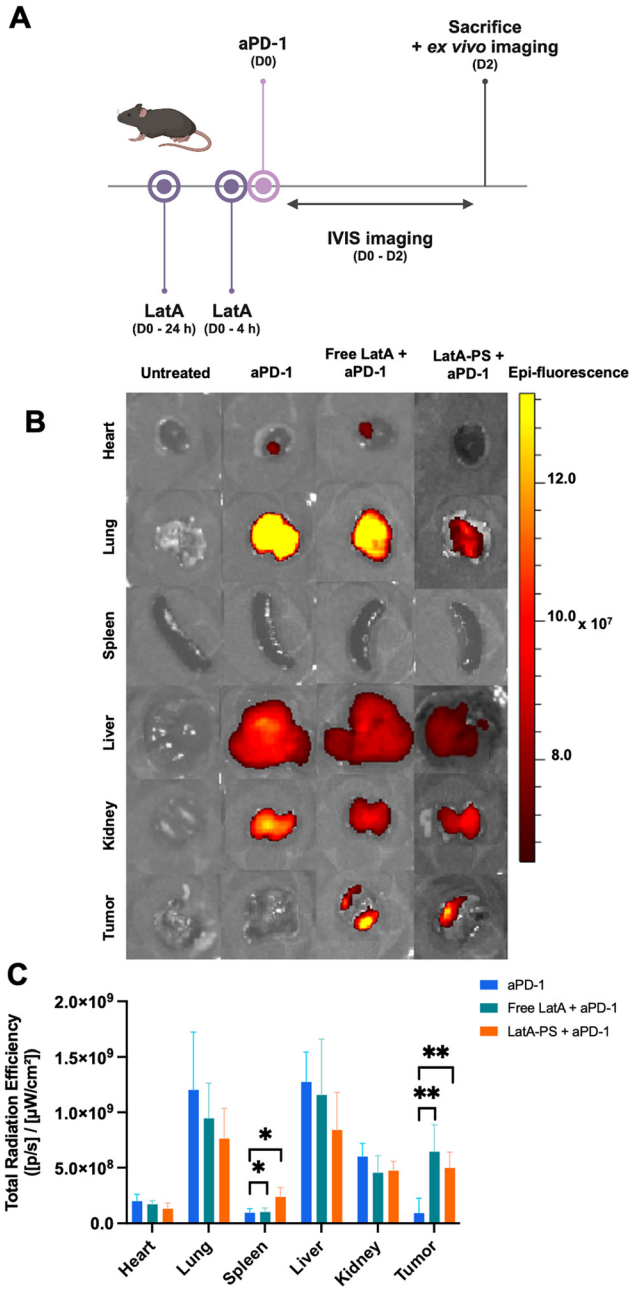

Fig. 2 Effect of LatA on organ-level biodistribution of aPD-1 in a murine melanoma model. (A) Mice bearing subcutaneous B16F10 tumors were administered two 7 µm injections of free LatA or LatA-PS 24 h (−24 h) and again 4 h (−4 h) prior to injection of 100 µg of Flamma® Fluors 648-labeled aPD-1. Untreated mice were used as controls. Mice were monitored with IVIS and sacrificed 2 days after the aPD-1 injection. (B) Representative *ex vivo* images of various tissues and (C) quantification are shown for aPD-1 accumulation in various tissues (n = 3–5). All data are reported as mean ± sd, * p-value < 0.05, ** p-value < 0.01 (ANOVA, see section Statistical analysis).

injections at both 24 h and 4 h prior to each aPD-1 administration (Fig. 3A). Untreated mice were used as controls. Mice were sacrificed 24 h after the final aPD-1 injection and flow cytometry was performed to determine the cellular biodistribution of aPD-1 in the tumor. Changes in the anticancer immune response were also analyzed in the tumor and spleen.

Since highly phagocytic cells can scavenge therapeutic antibodies, aPD-1 was expected to co-localize with myeloid cells in the TME.[36] Indeed, there was a distinct CD11b positive population in the tumor positive for Flamma® Fluors 648-labeled-aPD-1 by flow cytometry (Fig. S6A, ESI†). This CD11b positive cell engagement was lower in response to LatA priming, presumably due to inhibition of antibody uptake. This decline was significant in mice treated with LatA-PS, which reduced engagement 2-fold (Fig. 3B). Importantly, the decline in myeloid cell uptake was accompanied by an increase in target cell engagement. While PD-1 is expressed on a variety of cell types, T cells are considered to be the main driver of aPD-1's therapeutic activity.[37,38] LatA-PS priming significantly boosted the number of T cells in the tumor engaged with Flamma® Fluors 648-labeled-aPD-1, from 2.3 percent to 6.3 percent (Fig. 3C and Fig. S6B, ESI†). This can likely be attributed to the increased aPD-1 tumor accumulation (Fig. 2B and C), which would facilitate and increase T cell binding. The effect of LatA on the cellular-level biodistribution of aPD-1 was greatly enhanced by polymersome encapsulation. Since nanoparticles have increased uptake by the MPS, it is likely that LatA-PS more effectively targeted MPS cells than free LatA.[39] More efficient disabling of the system then resulted in greater changes in aPD-1 biodistribution. Overall, these results demonstrate that indirect targeting ameliorates both the organ-level and cellular-level biodistribution of aPD-1.

Indirect targeting enhances the anticancer immune response initiated by aPD-1

The decreased MPS uptake, increased tumor accumulation and elevated T cell engagement of aPD-1 translated to improvements in anticancer immunity. Flow cytometry indicated mice treated with aPD-1 monotherapy experienced lower levels of PD-1 expression on T cells in the spleen, suggesting less T cell exhaustion. These differences were only significant when combined with free LatA or LatA-PS (Fig. 3D).[38] As in the case of the T cell response, the innate immune response in the TME was heightened with indirect targeting. Flow cytometry indicated that there were ∼35 percent less CD163 positive macrophages in the tumor in response to LatA-PS priming (Fig. 3E). Free LatA priming resulted in a similar decline in the percent of CD163 positive macrophages, though this trend was not significant. CD163 is an important marker of macrophage polarization, indicating a more regenerative, less inflammatory phenotype.[40] Thus, lower, levels of CD163 positive macrophages suggests a more anti-cancer immune microenvironment. No significant differences from the untreated control were observed in mice that received the aPD-1 monotherapy alone.

To determine if the immune response was maintained over time, a second set of mice were treated with the same injection regimen and were sacrificed when tumor volumes reached 1000 mm^3 or at 40 days-post treatment initiation. The tumors were harvested, sectioned and stained for various markers. The tumor sections of these mice revealed significantly higher T cell infiltration in response to LatA-PS priming (Fig. 3F, I and Fig. S7, ESI†). Specifically, the CD3 signal in the tumor increased

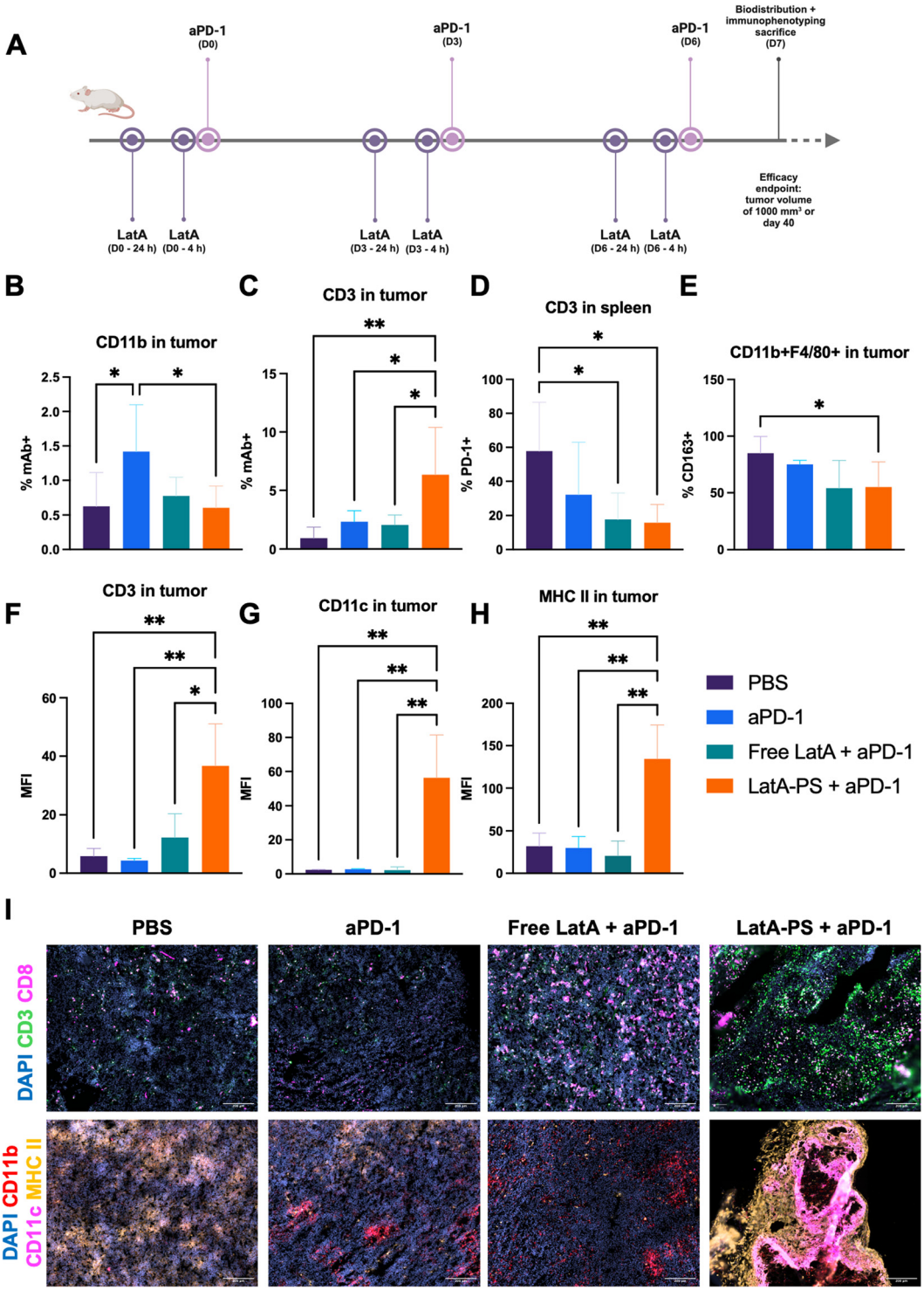

Fig. 3 Effect of LatA on cellular-level biodistribution of aPD-1 in a colon carcinoma model. Mice bearing subcutaneous CT26 tumors were treated with Flamma® Fluors 648-labeled aPD-1 at 10 mg kg^{-1} with or without 7 μm free LatA or LatA-PS. (A) Mice received three aPD-1 injections, separated by 3 days. LatA injections were given 24 h (−24 h) and 4 h (−4 h) prior to each aPD-1 injection. Untreated mice were used as controls. Mice were sacrificed 24 h after the final injection or at efficacy endpoints and flow cytometry of tumor tissue was performed (B–E, n = 5–6) and tumor tissues were stained (F–I, n = 3). aPD-1 engagement with (B) CD11b positive cells and (C) CD3 positive cells in the tumor. (D) PD-1 expression on CD3 positive cells in the spleen. (E) CD163 expression on CD11b positive F4/80 cells in the tumor. (F) CD3 (G) CD11c and (H) MHC II expression in the TME. (I) Representative immunofluorescence images of tumor sections. Scale bar represents 200 μm. All data are reported as mean ± sd, * p-value < 0.05, ** p-value < 0.01 (ANOVA, see section Statistical analysis).

3.2-, 8.5- and 6.3-fold in response to LatA-PS priming, compared to the free LatA-priming, aPD-1 monotherapy, or no treatment, respectively. Mice at efficacy endpoints also had a stronger myeloid cell presence in tumor tissues. Indirect targeting augmented CD11c expression in the TME (Fig. 3G, I, and Fig. S8, ESI†). That is, tumor tissues of mice primed with LatA-PS and treated with aPD-1, exhibited significantly higher CD11c expression than those of other groups, with an increase in MFI of over 25-fold for the LatA-PS group compared to all other groups. The CD11c positive cells appeared absent in some groups, as their presence was minimal in comparison to the strong CD11c signal in the LatA-PS primed group. Increasing the intensity of the CD11c group allows these cells to be more easily visualized but saturates the signal in the LatA-PS group (Fig. S8, ESI†). Differences in MHC II levels in the TME were similarly dramatic, with LatA-PS priming significantly

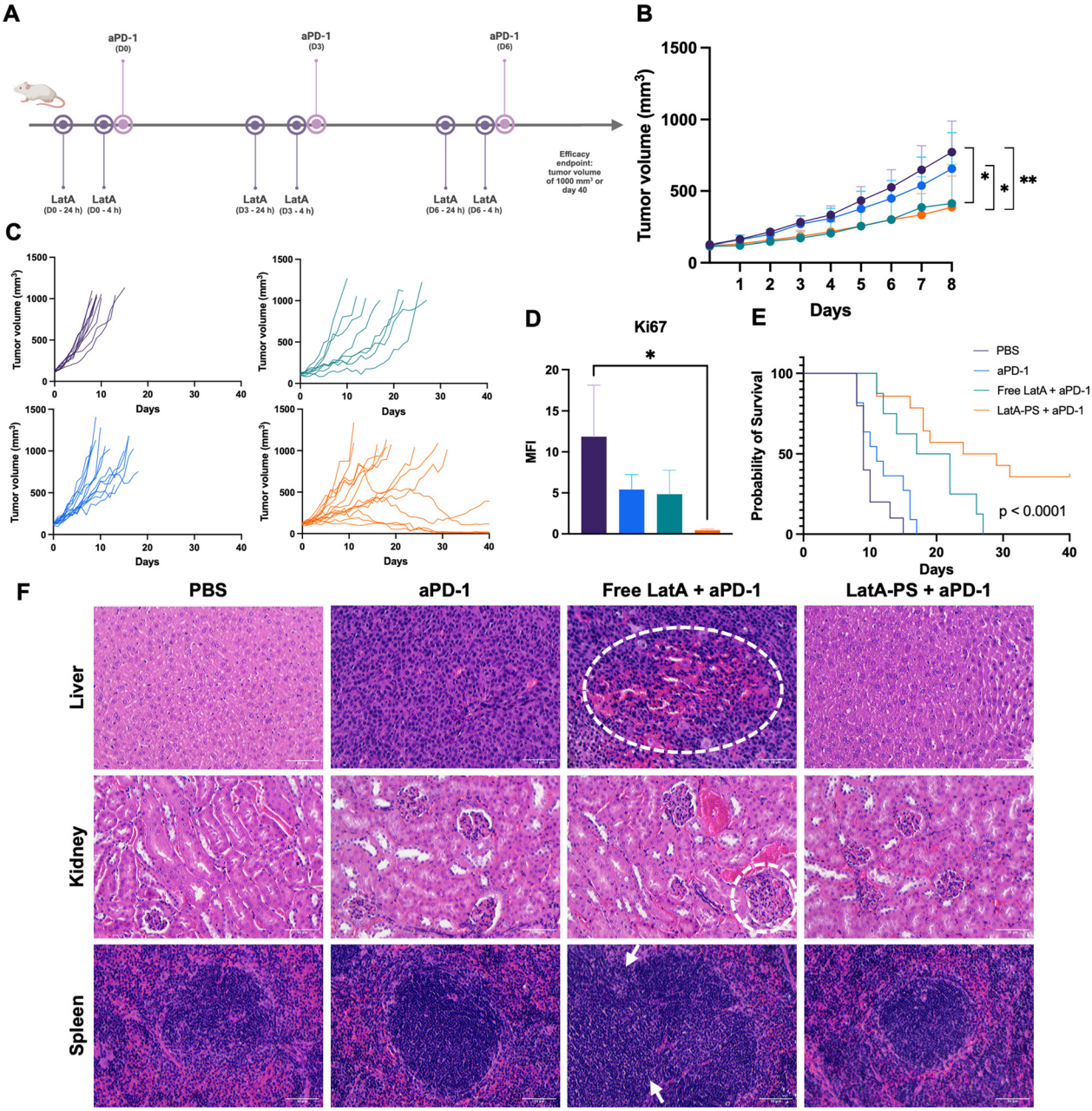

Fig. 4 Anticancer effect and safety of LatA and aPD-1 combination therapy on colon cancer *in vivo*. (A) Mice bearing subcutaneous CT26 tumors were divided into 4 groups and treated with either PBS, aPD-1, free LatA and aPD-1, or LatA-PS and aPD-1. aPD-1 injections were given at 10 mg kg^{-1}, once every 2 days for a total of three injections. Free LatA and LatA-PS injections occurred 24 h prior (−24 h) and again 4 h (−4 h) prior to each aPD-1 injection at a concentration of 7 μm. (B) Average tumor growth and over a period of 8 days (n = 8–14). (C) Individual tumor growth curves through day 40 post-treatment or until tumor volume exceeded 1000 mm^3. (D) Ki67 expression levels in tumor tissues (n = 3). (E) Survival of mice out to 40 days (n = 8–14). (F) Representative images of H&E staining of major organs (n = 3 technical replicates, n = 2 biological replicates). Scale bar represents 50 μm. All data are reported as mean ± sd, * p-value < 0.05, ** p-value < 0.01 (ANOVA, see section Statistical analysis).

increasing MHC II levels the TME 4.2- to 6.6-fold compared to all other groups (Fig. 3H, I and Fig. S8, ESI†). Collectively, these results indicate that indirect targeting enhances the anticancer immune response initiated by aPD-1 in a robust manner.

Indirect targeting enhances tumor growth inhibition in colon carcinoma

Since indirect targeting was found to improve aPD-1's accumulation in the tumor, engagement with T cells, and anticancer immune response, we anticipated it would also have a significant effect on tumor growth. To investigate this, mice were treated with the therapeutic dosing regimen described previously and tumors were allowed to grow until a volume of 1000 mm^3 or until 40 days after treatment initiation (Fig. 4A). We found that the anticancer efficacy of aPD-1, which had only a small impact on tumor growth inhibition when used alone, was enhanced with LatA priming. On day 8, the average tumor size of mice that received free LatA or LatA-PS were similar, paralleling the similar aPD-1 organ-level biodistribution results seen in Fig. 2 These tumors were significantly smaller than untreated mice, with 46.5 and 49.8 percent decreases in tumor volume, respectively (Fig. 4B, C and Fig. S9A, ESI†). This reduction in tumor volume in the LatA-PS group was also significant compared to the aPD-1 monotherapy group, with a 40.9 percent reduction in tumor volume comparatively. Furthermore, some mice treated with LatA-PS not only had slower growth, but also experienced reductions in tumor volume, a phenomenon that was not observed in any other group (Fig. 4C). The dynamics of tumor growth were confirmed on a cellular level, as the tumors of mice treated with aPD-1, with or without LatA priming, exhibited less Ki67 expression (Fig. 4D and Fig. S9B, ESI†). Ki67 is a marker of cellular proliferation, and thus tumors with lower Ki67 expression experienced slower growth. This difference was significant between the LatA-PS primed group and the untreated control, with a 27.5-fold decrease in MFI. Importantly, slower tumor growth translated to increased survival (Fig. 4E). Treatment with aPD-1 alone had a weak impact on survival, increasing median survival time from 9 to 11 days. The addition of free LatA or LatA-PS increased median survival time to 19.5 and 26.5 days, respectively, a significant improvement compared to the untreated and monotherapy groups. Notably, the LatA-PS group had significantly better survival than the free LatA group. This is consistent with the previous results showing polymersome encapsulation enhances LatA activity by increasing the engagement of aPD-1 with CD3 positive cells in the tumor (Fig. 3C). Additionally, the treatment was well-tolerated, with no significant changes in body weight observed during dosing (Fig. S9C, ESI†). Collectively, this data demonstrates that LatA priming can ameliorate the antitumor effects of aPD-1 and that indirect targeting is a promising strategy for improving therapeutic antibody efficacy.

Enhancing the activity of aPD-1 has important clinical implications. Perhaps the most significant consequence is that increasing the efficacy of a drug generally improves outcomes for the patient. Additionally, greater therapeutic activity could allow for reductions in dose, which can have several benefits. First, lowering the concentration of a pharmaceutical can reduce the likelihood and/or severity of adverse events that may lead to treatment discontinuation and failure in clinical trials.[29,41,42] Second, dosing frequency may be reduced, which can increase patient compliance and decrease healthcare costs, especially for therapeutics that require intravenous infusion.[43] Third, lower doses can increase affordability and accessibility of treatment. Thus, achieving enhanced therapeutic antibody efficacy with indirect targeting can be a tremendous benefit to the healthcare ecosystem.

LatA-PS increases safety of treatment *in vivo*

The safety of indirect targeting was further assessed with histological analysis. While no mice exhibited significant changes in body weight during treatment (Fig. S9C, ESI†), hematoxylin and eosin (H&E) staining of major organs indicated signs of toxicity for several groups receiving aPD-1. As broad disrupters of immune homeostasis, this is unfortunately common for ICIs. No signs of toxicity were noted in untreated mice (Fig. 4F and Fig. S9D, ESI†). Lymphocyte infiltration was seen in the livers of mice treated with aPD-1 alone, a phenomenon previously observed in response to ICI administration. The signs of toxicity apparent in the liver were intensified in mice primed with free LatA. Significant lymphocyte infiltration was observed in these tissues, as were signs of a hemorrhage, indicated by notable red blood cell accumulation in the tissue. While the aPD-1 monotherapy group also had red blood cell infiltration in the liver, only the change seen in the free LatA group is definitively pathological. The kidneys of mice primed with free LatA also showed signs of inflammation, with lymphocytes pooled in the left half of one of the glomeruli. Additionally, the spleens of these mice exhibited disrupted histoarchitecture. The follicular organization is disturbed, likely due to the presence of rapidly dividing immune cells resulting from aggressive inflammation.[44] LatA can be cytotoxic at high concentrations due to its interference with actin polymerization and is under investigation as an experimental chemotherapy since it can prevent cell division.[45] It is possible that since free LatA is toxic, it directly killed cells in the liver, kidney and spleen, and cell death contributed to the observed inflammation.[46]

The tissues of mice primed with LatA-PS lacked the signs of toxicity observed in those primed with free LatA. This difference is unlikely to be attributed solely to the subsequent aPD-1 injection, as LatA-PS resulted in lower aPD-1 accumulation in the liver than free form LatA, but not in the kidney and spleen (Fig. 2B and C). It is possible that this mitigated inflammation may be due to decreased LatA cytotoxicity upon polymersome encapsulation. Nanoparticle formulations can decrease the toxicity of free drugs, which was observed with LatA *in vitro* (Fig. 1C and D) and is consistent with our prior work using LatA-loaded nanocarriers.[22,47,48]

Incredibly, LatA-PS also reduced the toxicity associated with aPD-1. Hepatotoxicity is a known response to ICI treatment and is presumed to be due to a loss of self-tolerance.[28] Murine

models of ICI-related toxicity have implicated both T cells and myeloid cells in the liver inflammation.[29] Depletion of macrophages with clodronate liposomes has been shown to prevent anti-CD40-induced liver damage, suggesting the MPS plays a causal role in ICI-related hepatotoxicity.[49] In this work, we see a similar decrease in liver inflammation with indirect targeting, where LatA-PS priming seemingly reduces the liver toxicity in response to aPD-1 treatment. However, unlike clodronate liposomes, indirect targeting safely and temporarily disables pinocytosis without eliminating an entire cell population and broadly disrupting the immune microenvironment.[50]

The differences in toxicity observed in the liver may be the result of both organ- and cellular-level changes. It is possible that LatA-PS priming resulted in lower aPD-1 liver accumulation, which subsequentially decreased aPD-1-mediated toxicity (Fig. 2). Moreover, since ICIs can disrupt immune homeostasis, the resulting small modulations of immune cells can expand and propagate into wide ranging and often toxic effects. Depending on the immune mechanisms involved, these changes may not correlate directly with the concentration of aPD-1 in specific organs. These effects likely involve complex inflammatory pathways instead of direct cell killing and toxicity observed for chemotherapies.[13,28] Additionally, LatA may affect processes such as antigen presentation and receptor cycling, which rely on actin polymerization and modulate inflammatory responses.[51–53] The impact of indirect targeting on aPD-1 safety has important clinical implications, and additional work should be performed to elucidate how LatA-PS affect aPD-1-mediated off-target toxicity.

Compared to previously reported strategies, indirect targeting has the benefit of improving both therapeutic efficacy and safety without the need to modify antibody structure.[54] Antibody engineering can cause unwanted immunogenicity, which can result from changing the amino acid sequence, using nonmammalian cells for glycoengineering, or employing certain antibody drug conjugate linker methods. Furthermore, these approaches may decrease the affinity of the antibody for its intended target.[14,55] Changing the antibody structure can also be a cumbersome process, as a new design, in addition to screening, optimization and validation, is required for each target. Here, we describe an approach that employs a distinct stand-alone LatA-PS formulation, which avoids the need to modify the subsequently injected therapeutic antibody for improved delivery and efficacy, which may facilitate clinical translation. Additionally, its lack of reliance on antigen- or tissue-specific features, makes indirect targeting broadly applicable to other antibody-based therapeutics. As such, an interesting next testbed for this approach might be in ADC treatment, which can be severely limited by off-target toxicity. For example, indirect targeting can potentially reduce off-target chemotherapy uptake resulting from payload deconjugation or ADC uptake *via* pinocytosis, two processes that contribute to off-target toxicity.[13]

To further enhance the clinical relevance of the indirect targeting platform, additional injection regimes can be explored. The time points and route of administration selected here were based on an established scheme to ameliorate nanoparticle delivery. In the previous work, two dosing schedules were tested.[18] The first had a 24 h and 4 h pre-injection of LatA prior to the effector nanoparticle administration. The other platform had a 24 h pre-injection of LatA followed by a co-injection of LatA with the effector nanoparticle. Here, we chose to match the 24 h and 4 h pre-injection regimen. PEG-*b*-PPS polymersome accumulation is noticeable in MPS tissues such as the liver, kidney and spleen in as little as 1 h after intravenous injection and continues to have significant accumulation through at least 48 h.[27] We wanted to ensure the nanoparticles had sufficient time to accumulate and exert their effects on macropinocytosis before administering the antibody. Additionally, the effects of LatA on endocytosis inhibition start in as little as 30 min and begin to wane between 1 and 2 h *in vitro*, but still have significant effects for at least 2 h (Fig. S4, ESI†).[27] Thus, we hypothesized that the established pre-treatment strategy would have a positive effect on aPD-1 biodistribution. As this work is a proof-of-concept demonstrating the impact of LatA priming on aPD-1 therapeutic activity, additional dosing regimens were not evaluated. Exploring a co-injection strategy, in which LatA and aPD-1 are administered simultaneously, may be more translatable to the clinic, as it would require fewer intravenous infusions. Instead of using the intravenous route, more easily administered subcutaneous injections of LatA might also be of benefit for clinical translation. Regardless, this work highlights the ability of indirect targeting to improve both the safety and efficacy of aPD-1 administration.

Conclusions

In this work, a new indirect targeting strategy was developed to enhance the delivery of therapeutic antibodies to solid tumors. Priming with pinocytosis inhibitory LatA-PS was shown to improve the biodistribution of aPD-1 by decreasing accumulation within the MPS, enhancing tumor accumulation, and increasing interaction with T cells. This change in biodistribution translated to meaningful benefits in the anticancer immune response and tumor growth inhibition initiated by aPD-1. Furthermore, this approach improved the safety of aPD-1 by minimizing its off-target toxicity. This enhanced efficacy and reduced off-target toxicity may result in many benefits in the clinic, including better prognosis, fewer adverse events, less frequent dosing, greater patient compliance and lower cost.[41,43,56] Given its ability to augment both efficacy and safety, antigen- and tissue-agonistic approach, and capacity to complement other targeting strategies, we anticipate that indirect targeting *via* LatA-PS will improve a wide variety of therapeutic antibodies across solid tumors and for diverse disease indications.

Experimental sections

Study design

The goal of this work was to determine how changing the biodistribution of aPD-1 to prevent its uptake by the MPS affected its anticancer response. To do this, we formed LatA-

loaded nanoparticles to inhibit the MPS. We explored their effect on actin polymerization and aPD-1 cellular uptake *in vitro*, and how they change aPD-1 organ- and cellular level biodistribution *in vivo*. We investigated their ability to enhance aPD-1's anticancer immune response and tumor growth inhibition. Finally, we evaluated the toxicity of the approach.

Materials

LatA and was Phalloidin-iFluor™ 488 Conjugate were purchased from Cayman Chemicals. Anti-Mouse PD-1 (CD279) Rat Monoclonal Antibody [RMP1–14] was purchased from Bio X Cell. Flamma® Fluors 648 was purchased from BioActs. Zeba spin desalting columns, NucBlue™ and dialysis cassettes were purchased from ThermoFisher. DMEM was purchased from Gibco. Collagenase III and liberase TH and were purchased from Worthington Biomedical and Roche, respectively. Zombie live/dead, red blood cell lysis buffer, cell staining buffer, fluorescent antibodies and cell fixation buffer were purchased from BioLegend. All other chemicals were purchased from Sigma-Aldrich.

Cell culture

Murine colon carcinoma CT26 cells, melanoma B16F10 cells, and RAW 264.7 macrophages were purchased from ATCC. CT26 and DC2.4 cells were cultured in complete media, consisting of RMPI 1640 with 10% FBS, 100 U mL^{-1} and 100 μg mL^{-1} streptomycin. Murine B16F10 cells and RAW 264.7 macrophages cells were purchased from ATCC. Raw 264.7 cells were cultured in DMEM media with 10% FBS, 100 U mL^{-1} and 100 μg mL^{-1} streptomycin. Cells were utilized in experiments during the logarithmic growth phase.

Animals

Female C57BL/6 mice (6–8 weeks old) were purchased from Jackson Laboratories. Male Balb/c mice (6–8 weeks old) were purchased from Jackson Laboratories. All animal experiments were conducted in accordance with the guidelines and regulations approved by the Laboratory Animal Welfare and Ethics Committee of Northwestern University (Approved Protocol Numbers: IS00017606 and IS00007992).

Synthesis and characterization PEG-*b*-PPS-Bz

PEG_{17}-*b*-PPS_{30}-Bz was synthesized according to established procedures.[26] Methyl ether PEG was functionalized with a mesylate group *via* the addition of sodium hydroxide and methanesulfonyl chloride. PEG mesylate was then used to generate PEG thioacetate. Finally, PEG thioacetate was used to initiate the living polymerization of propylene sulfide, which was end capped with benzyl bromide. ^{1}H NMR spectroscopy and GPC were used to characterize the synthesized polymer.

Preparation of polymersomes by thin film hydration

To prepare polymersomes, PEG_{17}-*b*-PPS_{30}-Bz (10 mg) was measured and placed in a sterile 2 mL glass vial and dissolved in THF (200 μL). LatA (10 μg) was dissolved in THF (100 μL) and then combined with the polymer. The THF was removed *via* desiccation and the polymer deposit was rehydrated with PBS solution (1 mL, pH 7.4). The sample was shaken overnight at RT. Unencapsulated drug was removed by filtering samples with a Zeba spin desalting column (7 KD MWCO, 0.5 mL). Debris and nanoparticle aggregates were removed by filtering through a PTFE filter (0.2 μm, 14 mm).

Physiochemical properties

Polymersome size and zeta potential were determined with dynamic light scattering (DLS, Zetasizer, Malvern, UK). Samples were prepared by diluting PS formulations (0.1–0.3 mg) in PBS (1 mL, pH 7.4) using a disposable low-volume sample cuvette. Particle morphology was visualized using cryogenic transmission electron microscopy (TEM, JEOL 1400 Flash,120 kV, JAPAN) and a Gatan OneView 4k camera. Nanostructure morphology was further confirmed by small angle X-ray scattering, which was performed at Argonne National Laboratories. Data reduction/buffer subtraction and model fitting were performed using the BioXTAS RAW 2.8.3 and SasView 5.0.5 software, respectively.[57] Vesicle sphere models were used to fit the data.

Quantification of LatA loading using HPLC

To determine LatA drug loading, aliquots of LatA-loaded PS (0.1 mg) were dried under vacuum. The resulting solid was resuspended in 95% 100 μL methanol and sonicated for 5 min. The sample was placed at −80 °C for 6 h and centrifuged at 170 00*g* at 9 °C for 10 min. The supernatant was removed and the pellet was resuspended in 95% methanol and placed at −20 °C for 1 h. The solution was spun at 17 000*g* at −9 °C for 10 min. The supernatants from each spin were combined for analysis. The concentration of LatA was determined with RP-HPLC. HPLC was performed using a C18 column (Avantor) and methanol/water gradient for the mobile phase. Absorbance values were determined at 235 nm and LatA concentration was determined with a LatA calibration curve in methanol.

Labeling of aPD-1 with Flamma® Fluors 648

Flamma® Fluors 648 was dissolved in DMSO (1 mg, 100 μL). APD-1 was dissolved in reaction buffer (500 mM carbonate, pH 9.5). The dye was slowly added to the aPD-1 solution and allowed to stir for 1 h at RT. The solution was dialyzed against water (20 KD MWCO, 12 mL) to remove any unconjugated dye.

Cytotoxicity in colon carcinoma cells and macrophages with MTT

The cytotoxicity of free LatA and LatA-PS was evaluated using an MTT assay. Briefly, CT26 cells or RAW 264.7 macrophages were seeded on a 96-well plate (6×10^4 cells $well^{-1}$) and allowed to adhere overnight. Cells were treated with complete media, free LatA (100 μL, 0.05, 0.5, 1, 2, 4 or 7 μM LatA) or LatA-PS (100 μL, 0.05, 0.5, 1, 2, 4 or 7 μM LatA) for 24 h. After incubation, the cells were washed and treated with MTT (100 μL, 0.4 mg mL^{-1}) for 4 h. Then the media was removed and 150 μL DMSO was added to each well. Absorbance was detected at 630 nm (A_{630}) and 570 nm (A_{570}). Viability was calculated with the formula:

viability (%) = (A_{630} − A_{570} of treated cells/A_{630} − A_{570} of untreated cells) × 100%.

Cytotoxicity in colon carcinoma cells and macrophages with flow cytometry

The cytotoxicity of free LatA and LatA-PS was evaluated in RAW 264.7 macrophages by flow cytometry. RAW 264.7 macrophages were incubated with complete media, free LatA (100 μL, 0.01, 0.1, 1, or 10 μM) or LatA-PS (100 μL, 0.01, 0.1, 1, or 10 μM) for 24 h. Cells were collected and stained with Zombie NIR (1 μL in 1000 μL of cell staining buffer) for 15 min at RT. Flow cytometry was run (Aurora 3L, Cytek, USA) and the percentage of Zombie NIR-negative cells of singlets were determined with FlowJo™ software version 10.10. The percentage of Zombie-negative cells corresponded to cellular viability.

Kinetics of LatA-PS pinocytosis inhibition

To determine when the effects of LatA-PS on pinocytosis start, DC2.4 cells were incubated cells with LatA-PS (2 μM) for 0.5 h and then with DiD-loaded polymersomes (DiD-PS) at the same polymer concentration for 6 h. To determine how long the effects of LatA-PS last, DC2.4 cells were incubated cells with LatA-PS (2 μM) for 2 h, allowed to recover for 0 h, 1 h or 2 h, and then incubated with DiD-PS for 6 h. Cellular uptake was measured *via* DiD fluorescence using flow cytometry. Data was analyzed using the FlowJo™ software version 10.10.

Effect of LatA on actin polymerization *in vitro* with confocal microscopy

The effect of Lat A-PS on cells on actin polymerization was investigated with confocal microscopy. 3×10^5 RAW 264.7 cells were seeded on a 35 mm dish and incubated for 24 hours at 37 °C and 5.0% CO_2. Cells were treated with Lat A-PS (7 μM) for 24 hours. Cells were fixed with 4% formaldehyde solution (15 min, RT). Then cells were washed and permeabilized with 0.5% Triton X-100 (15 min, RT). Cells were blocked with 3% bovine serum albumin (BSA) overnight prior to staining. To stain F-actin, cells were incubated with Alexa 488-Phalloidin diluted 1000× in 1% BSA (20 min, RT). Cells were washed with PBS and stained with NucBlue (1 drop mL^{-1} media, 30 min, RT). Cells were washed again with fresh CDMEM and imaged with Nikon Super-resolution by Optical Re-assignment (SoRa) Spinning-disk Confocal System. Images were collected with a 60× oil immersion objective magnification lens was used with SoRa obtaining final magnification of 168×. The image was analyzed with NIS elements imaging software version 5.41.02.

Effect of LatA on aPD-1 engagement *in vitro*

The effect of LatA-PS on aPD-1 engagement with RAW 264.7 macrophages was investigated. Briefly, 8.1×10^5 cells were seeded on a 48-well plate and incubated for 24 h. Cells were then treated with either 7 μM LatA, 1 μM LatA or PBS for 24 h. Cells were washed and then incubated with Flamma® Fluors 648-labeled-aPD-1 (12.5 μg mL^{-1}) for 2 h. Cells were washed to remove aPD-1 in solution and the fluorescence was (λ_{ex}: 646 nm λ_{em}: 648 nm) measured to approximate aPD-1 engagement with cells.

Uptake of aPD-1 *in vitro* with confocal microscopy

RAW 264.7 macrophages were seeded on a 4-well confocal dish (2×10^5 cells $well^{-1}$) and allowed to adhere overnight. Cells were treated with complete media, free LatA (500 μL, μM) or LatA-PS (500 μL, 2 μM) for 30 min. After incubation, the cells were washed and treated with Flamma® Fluors 648-labeled-aPD-1 (500 μL, 16 μM) for 15 min. Then the cells were washed and stained with NucBlue (1 drop mL^{-1}) for 15 min. Confocal microscopy was performed (SP8, Leica, Germany) with a 63× oil immersion objective magnification lens.

aPD-1 organ-level biodistribution in cancer-bearing mice

To establish murine melanoma, mice were injected subcutaneously with B16F10 cells (5×10^5) in the right hind flank. Tumors were allowed to grow until ~100 mm^3 at which point mice received a single 100 μg intravenous injection of Flamma® Fluors 648-labeled-aPD-1. Mice in LatA-PS or free LatA groups received two intravenous LatA doses (7 μM, 100 μL) 24 h and again 4 h prior to the aPD-1 injection. Tumor size was measured with calipers ($V = 0.5LW^2$, where W is the shorter perpendicular distance). aPD-1 tumor accumulation was measured with IVIS at 1 h, 12 h, 24 h, and 48 h after aPD-1 accumulation. Imaging angle was optimized to facilitate measuring tumor uptake in real time. Mice were sacrificed 48 h post-injection and *ex vivo* imaging of the heart, lung, spleen, liver, kidney and tumor was performed. Images were analyzed with the Living Image® software. For quantification, background elimination was performed by subtracting the average total radiant efficiency of untreated mice from each respective organ.

aPD-1 cellular-level biodistribution and immunophenotyping in cancer-bearing mice

To establish colon carcinoma, mice were injected subcutaneously with CT26 cells (2×10^5) in the right hind flank. Tumors were allowed to grow until ~120 mm^3 at which point treatment with Flamma® Fluors 648-labeled-aPD-1 (10 mg kg^{-1}) or a saline control was initiated. For all experiments, mice received 3 intraperitoneal aPD-1 injections, separated by 3 days. Mice in LatA-PS or free LatA groups received intravenous LatA injections (7 μM, 100 μL) 24 h and again 4 h prior to each aPD-1 injection. Tumor size was measured with calipers ($V = 0.5LW^2$, where W is the shorter perpendicular distance). One day after the final treatment the mice were sacrificed. The spleens and tumors were excised. Tumors were minced and digested with 600 μL of Collagenase III (3000 units mL^{-1} in HBSS) or 400 μL of Liberase TH and 100 Kunitz units of DNase I. Then, single cell suspensions were generated by passing the digested tumor tissue and spleen through a 70 μm cell strainer. Red blood cells were removed with RBC lysis buffer (5 min, 4 °C). The harvested cells were stained with various antibodies to analyze with flow cytometry (Aurora 3L, Cytek, USA). Data analysis was performed FlowJo™ software version 10.10.

Tumor growth inhibition

A CT26 model was established, and treatment was performed as described above, though unlabeled aPD-1. Body weight and tumor size were observed daily. Mice were sacrificed when tumors were 1000 mm^3 or at 40 days after treatment began, whichever came first. In some cases, the tumor and major organs were collected for further analysis.

Tumor spatial phenotyping

Tumors were excised from mice at efficacy endpoints and embedded in OCT solution prior to freezing at −80 °C. Samples were sectioned, stained and imaged with a PhenoCycler-Fusion. Samples were analyzed using the QuPath software version 0.5.1. The DAPI signal of some Ki67 images were enhanced to normalize signal background.

Safety analysis

The heart, lungs, liver, kidney and spleen from mice at efficacy endpoints were fixed in 10% neutral buffered formalin and embedded in paraffin prior to section. Hematoxylin and eosin staining was performed to evaluate organ-specific toxicity.

Statistical analysis

Statistics were performed using a one-way ANOVA and Tukey's multiple comparison test using the software GraphPad Prism version 10.4.1. Statistical significance was determined if the p-value was below 0.05. * p-value < 0.05, ** p-value < 0.01, *** p-value < 0.001, **** p-value < 0.001.

Abbreviations

ADC	Antibody–drug–conjugate
aPD-1	Anti-programmed death receptor-1
FcR	Fc receptor
FcRn	Neonatal Fc receptor
ICI	Immune checkpoint inhibitor
IVIS	*In vivo* imaging system
LatA	Latrunculin A
LatA-PS	LatA-loaded polymersome
MFI	Mean fluorescence intensity
MPS	Mononuclear phagocyte system
PEG-*b*-PPS-Bz	Poly(ethylene glycol)-*b*-poly(propylene sulfide)-benzyl
SAXS	Small angle X-ray scattering
RP-HPLC	Reverse-phase high performance liquid chromatography
TME	Tumor microenvironment

Author contributions

S. R. Z. and H. P. designed the research with input from W. Q., G. L., E. S. and B. Z. S. R. Z. and H. P. performed experiments with the assistance of W. Q., G. L., S. A., S. H. S., D. B. S., J. L. and R. W. R. S. R. Z. and E. S. wrote and revised the manuscript. All authors have given approval to the final version of the manuscript.

Data availability

The authors confirm that the data supporting the findings of this work is available within the article. The raw data is also accessible from the corresponding author upon reasonable request.

Conflicts of interest

There are no conflicts to declare.

Acknowledgements

This work was funded through NIH T32GM008449. CyroTEM was done by Eric Roth of the BioCryo Core. Confocal imaging was performed in the Biological Imaging Facility at Northwestern University (RRID:SCR_017767). Animal experiments were carried out with the assistance of the Developmental Therapeutics Core (RRID:SCR_017948). IVIS work was performed at the Northwestern University Center for Advanced Molecular Imaging (RRID:SCR_021192). Tumor tissue sectioning and PhenoCycler imaging were performed by the Immunotherapy Assessment Core. Histology was performed by the Mouse Histology & Phenotyping Laboratory. Figures were made with BioRender.

References

1 C. Mattiuzzi and G. Lippi, Current Cancer Epidemiology, *J. Epidemiol. Glob. Health*, 2019, **9**(4), 217–222, DOI: **10.2991/jegh.k.191008.001**.
2 G. P. Adams and L. M. Weiner, Monoclonal Antibody Therapy of Cancer, *Nat. Biotechnol.*, 2005, **23**(9), 1147–1157, DOI: **10.1038/nbt1137**.
3 E. Cruz and V. Kayser, Monoclonal Antibody Therapy of Solid Tumors: Clinical Limitations and Novel Strategies to Enhance Treatment Efficacy, *Biol.: Targets Ther.*, 2019, **13**, 33–51, DOI: **10.2147/BTT.S166310**.
4 R. E. Kontermann, Strategies to Extend Plasma Half-Lives of Recombinant Antibodies, *BioDrugs*, 2009, **23**(2), 93–109, DOI: **10.2165/00063030-200923020-00003**.
5 A. Shah, S. Rauth, A. Aithal, S. Kaur, K. Ganguly, C. Orzechowski, G. C. Varshney, M. Jain and S. K. Batra, The Current Landscape of Antibody-Based Therapies in Solid Malignancies, *Theranostics*, 2021, **11**(3), 1493–1512, DOI: **10.7150/thno.52614**.
6 M. Ovacik and K. Lin, Tutorial on Monoclonal Antibody Pharmacokinetics and Its Considerations in Early Development, *Clin. Transl. Sci.*, 2018, **11**(6), 540–552, DOI: **10.1111/cts.12567**.
7 A. V. Kamath, Translational Pharmacokinetics and Pharmacodynamics of Monoclonal Antibodies, *Drug Discovery Today Technol.*, 2016, **21–22**, 75–83, DOI: **10.1016/j.ddtec.2016.09.004**.
8 B. M. Bordeau and J. P. Balthasar, Strategies to Enhance Monoclonal Antibody Uptake and Distribution in Solid Tumors, *Cancer Biol. Med.*, 2021, **18**(3), 649–664, DOI: **10.20892/j.issn.2095-3941.2020.0704**.

9 T. Kurino, R. Matsuda, A. Terui, H. Suzuki, T. Kokubo, T. Uehara, Y. Arano, A. Hisaka and H. Hatakeyama, Poor Outcome with Anti-Programmed Death-Ligand 1 (PD-L1) Antibody Due to Poor Pharmacokinetic Properties in PD-1/PD-L1 Blockade-Sensitive Mouse Models, *J. Immunother. Cancer*, 2020, **8**(1), e000400, DOI: **10.1136/jitc-2019-000400**.

10 A. Chow, B. D. Brown and M. Merad, Studying the Mononuclear Phagocyte System in the Molecular Age, *Nat. Rev. Immunol.*, 2011, **11**(11), 788–798, DOI: **10.1038/nri3087**.

11 C. Halma, M. R. Daha and L. A. Van Es, *In Vivo* Clearance by the Mononuclear Phagocyte System in Humans: An Overview of Methods and Their Interpretation, *Clin. Exp. Immunol.*, 2008, **89**(1), 1–7, DOI: **10.1111/j.1365-2249.1992.tb06868.x**.

12 H. H. Gustafson, D. Holt-Casper, D. W. Grainger and H. Ghandehari, Nanoparticle Uptake: The Phagocyte Problem, *Nano Today*, 2015, **10**(4), 487–510, DOI: **10.1016/j.nantod.2015.06.006**.

13 T. D. Nguyen, B. M. Bordeau and J. P. Balthasar, Mechanisms of ADC Toxicity and Strategies to Increase ADC Tolerability, *Cancers*, 2023, **15**(3), 713, DOI: **10.3390/cancers15030713**.

14 T. Igawa, H. Tsunoda, T. Tachibana, A. Maeda, F. Mimoto, C. Moriyama, M. Nanami, Y. Sekimori, Y. Nabuchi, Y. Aso and K. Hattori, Reduced Elimination of IgG Antibodies by Engineering the Variable Region, *Protein Eng., Des. Sel.*, 2010, **23**(5), 385–392, DOI: **10.1093/protein/gzq009**.

15 P. J. Carter and V. Quarmby, Immunogenicity Risk Assessment and Mitigation for Engineered Antibody and Protein Therapeutics, *Nat. Rev. Drug Discovery*, 2024, **23**(12), 898–913, DOI: **10.1038/s41573-024-01051-x**.

16 C. Sheridan, Pancreatic Cancer Provides Testbed for First Mechanotherapeutics, *Nat. Biotechnol.*, 2019, **37**(8), 829–831, DOI: **10.1038/d41587-019-00019-2**.

17 J. Zalevsky, A. K. Chamberlain, H. M. Horton, S. Karki, I. W. L. Leung, T. J. Sproule, G. A. Lazar, D. C. Roopenian and J. R. Desjarlais, Enhanced Antibody Half-Life Improves in Vivo Activity, *Nat. Biotechnol.*, 2010, **28**(2), 157–159, DOI: **10.1038/nbt.1601**.

18 T. Stack, Y. Liu, M. Frey, S. Bobbala, M. Vincent and E. Scott, Enhancing Subcutaneous Injection and Target Tissue Accumulation of Nanoparticles *via* Co-Administration with Macropinocytosis Inhibitory Nanoparticles (MiNP), *Nanoscale Horiz.*, 2021, **6**(5), 393–400, DOI: **10.1039/D0NH00679C**.

19 M. P. Vincent, J. O. Navidzadeh, S. Bobbala and E. A. Scott, Leveraging Self-Assembled Nanobiomaterials for Improved Cancer Immunotherapy, *Cancer Cell*, 2022, **40**(3), 255–276, DOI: **10.1016/j.ccell.2022.01.006**.

20 E. Munari, F. R. Mariotti, L. Quatrini, P. Bertoglio, N. Tumino, P. Vacca, A. Eccher, F. Ciompi, M. Brunelli, G. Martignoni, G. Bogina and L. Moretta, PD-1/PD-L1 in Cancer: Pathophysiological, Diagnostic and Therapeutic Aspects, *Int. J. Mol. Sci.*, 2021, **22**(10), 5123, DOI: **10.3390/ijms22105123**.

21 W. Zhong, J. S. Myers, F. Wang, K. Wang, J. Lucas, E. Rosfjord, J. Lucas, A. T. Hooper, S. Yang, L. A. Lemon, M. Guffroy, C. May, J. R. Bienkowska and P. A. Rejto, Comparison of the Molecular and Cellular Phenotypes of Common Mouse Syngeneic Models with Human Tumors, *BMC Genomics*, 2020, **21**(1), 2, DOI: **10.1186/s12864-019-6344-3**.

22 T. Stack, M. Vincent, A. Vahabikashi, G. Li, K. M. Perkumas, W. D. Stamer, M. Johnson and E. Scott, Targeted Delivery of Cell Softening Micelles to Schlemm's Canal Endothelial Cells for Treatment of Glaucoma, *Small*, 2020, **16**(43), 2004205, DOI: **10.1002/smll.202004205**.

23 J. A. Burke, X. Zhang, S. Bobbala, M. A. Frey, C. Bohorquez Fuentes, H. Freire Haddad, S. D. Allen, R. A. K. Richardson, G. A. Ameer and E. A. Scott, Subcutaneous Nanotherapy Repurposes the Immunosuppressive Mechanism of Rapamycin to Enhance Allogeneic Islet Graft Viability, *Nat. Nanotechnol.*, 2022, **17**(3), 319–330, DOI: **10.1038/s41565-021-01048-2**.

24 A. E. Nel, L. Mädler, D. Velegol, T. Xia, E. M. V. Hoek, P. Somasundaran, F. Klaessig, V. Castranova and M. Thompson, Understanding Biophysicochemical Interactions at the Nano–Bio Interface, *Nat. Mater.*, 2009, **8**(7), 543–557, DOI: **10.1038/nmat2442**.

25 I. V. Zelepukin, K. G. Shevchenko and S. M. Deyev, Rediscovery of Mononuclear Phagocyte System Blockade for Nanoparticle Drug Delivery, *Nat. Commun.*, 2024, **15**(1), 4366, DOI: **10.1038/s41467-024-48838-5**.

26 E. A. Scott, A. Stano, M. Gillard, A. C. Maio-Liu, M. A. Swartz and J. A. Hubbell, Dendritic Cell Activation and T Cell Priming with Adjuvant- and Antigen-Loaded Oxidation-Sensitive Polymersomes, *Biomaterials*, 2012, **33**(26), 6211–6219, DOI: **10.1016/j.biomaterials.2012.04.060**.

27 S. Yi, S. D. Allen, Y.-G. Liu, B. Z. Ouyang, X. Li, P. Augsornworawat, E. B. Thorp and E. A. Scott, Tailoring Nanostructure Morphology for Enhanced Targeting of Dendritic Cells in Atherosclerosis, *ACS Nano*, 2016, **10**(12), 11290–11303, DOI: **10.1021/acsnano.6b06451**.

28 D. Remash, D. S. Prince, C. McKenzie, S. I. Strasser, S. Kao and K. Liu, Immune Checkpoint Inhibitor-Related Hepatotoxicity: A Review, *World J. Gastroenterol.*, 2021, **27**(32), 5376–5391, DOI: **10.3748/wjg.v27.i32.5376**.

29 K. Adam, A. Iuga, A. S. Tocheva and A. Mor, A Novel Mouse Model for Checkpoint Inhibitor-Induced Adverse Events, *PLoS One*, 2021, **16**(2), e0246168, DOI: **10.1371/journal.pone.0246168**.

30 H. Konishi, S. Kikuchi, T. Ochiai, H. Ikoma, T. Kubota, D. Ichikawa, H. Fujiwara, K. Okamoto, C. Sakakura, T. Sonoyama, Y. Kokuba, H. Sasaki, T. Matsui and E. Otsuji, Latrunculin a Has a Strong Anticancer Effect in a Peritoneal Dissemination Model of Human Gastric Cancer in Mice, *Anticancer Res.*, 2009, **29**(6), 2091–2097.

31 Latrunculins—Novel Marine Macrolides That Disrupt Microfilament Organization and Affect Cell Growth: I. Comparison with Cytochalasin D.

32 T. Stack, A. Vahabikashi, M. Johnson and E. Scott, Modulation of Schlemm's Canal Endothelial Cell Stiffness via Latrunculin Loaded Block Copolymer Micelles, *J. Biomed. Mater. Res., Part A*, 2018, **106**(7), 1771–1779, DOI: **10.1002/jbm.a.36376**.

33 A. Geraud, P. Gougis, A. Vozy, C. Anquetil, Y. Allenbach, E. Romano, E. Funck-Brentano, J. J. Moslehi, D. B. Johnson and J.-E. Salem, Clinical Pharmacology and Interplay of Immune Checkpoint Agents: A Yin-Yang Balance, *Annu.*

Rev. Pharmacol. Toxicol., 2021, **61**(1), 85–112, DOI: **10.1146/annurev-pharmtox-022820-093805**.

34 M. G. Lechner, S. S. Karimi, K. Barry-Holson, T. E. Angell, K. A. Murphy, C. H. Church, J. R. Ohlfest, P. Hu and A. L. Epstein, Immunogenicity of Murine Solid Tumor Models as a Defining Feature of in Vivo Behavior and Response to Immunotherapy, *J. Immunother.*, 2013, **36**(9), 477–489, DOI: **10.1097/01.cji.0000436722.46675.4a**.

35 C. S. Lobo, M. I. P. Mendes, D. A. Pereira, L. C. Gomes-da-Silva and L. G. Arnaut, Photodynamic Therapy Changes Tumour Immunogenicity and Promotes Immune-Checkpoint Blockade Response, Particularly When Combined with Micromechanical Priming, *Sci. Rep.*, 2023, **13**(1), 11667, DOI: **10.1038/s41598-023-38862-8**.

36 F. Davodabadi, S. F. Sajjadi, M. Sarhadi, S. Mirghasemi, M. Nadali Hezaveh, S. Khosravi, M. Kamali Andani, M. Cordani, M. Basiri and S. Ghavami, Cancer Chemotherapy Resistance: Mechanisms and Recent Breakthrough in Targeted Drug Delivery, *Eur. J. Pharmacol.*, 2023, **958**, 176013, DOI: **10.1016/j.ejphar.2023.176013**.

37 S. Simon and N. Labarriere, PD-1 Expression on Tumor-Specific T Cells: Friend or Foe for Immunotherapy?, *OncoImmunology*, 2018, **7**(1), e1364828, DOI: **10.1080/2162402X.2017.1364828**.

38 J. Lee, E. Ahn, H. T. Kissick and R. Ahmed, Reinvigorating Exhausted T Cells by Blockade of the PD-1 Pathway, *Forum Immunopathol. Dis. Ther.*, 2015, **6**(1–2), 7–17, DOI: **10.1615/ForumImmunDisTher.2015014188**.

39 D. J. Irvine, M. C. Hanson, K. Rakhra and T. Tokatlian, Synthetic Nanoparticles for Vaccines and Immunotherapy, *Chem. Rev.*, 2015, **115**(19), 11109–11146, DOI: **10.1021/acs.chemrev.5b00109**.

40 Z. Wei, Z. Zhang, T. Yong, N. Bie, G. Zhan, X. Li, Q. Liang, J. Li, J. Yu, G. Huang, Y. Yan, Z. Zhang, B. Zhang, G. Lu, B. Huang and X. Yang, Boosting Anti-PD-1 Therapy with Metformin-Loaded Macrophage-Derived Microparticles, *Nat. Commun.*, 2021, **12**, 440–460, DOI: **10.1038/s41467-020-20723-x**.

41 C. G. Daughton and I. S. Ruhoy, Lower-Dose Prescribing: Minimizing ''Side Effects'' of Pharmaceuticals on Society and the Environment, *Sci. Total Environ.*, 2013, **443**, 324–337, DOI: **10.1016/j.scitotenv.2012.10.092**.

42 T. T. Hansel, H. Kropshofer, T. Singer, J. A. Mitchell and A. J. T. George, The Safety and Side Effects of Monoclonal Antibodies, *Nat. Rev. Drug Discovery*, 2010, **9**(4), 325–338, DOI: **10.1038/nrd3003**.

43 M. Viola, J. Sequeira, R. Seiça, F. Veiga, J. Serra, A. C. Santos and A. J. Ribeiro, Subcutaneous Delivery of Monoclonal Antibodies: How Do We Get There?, *J. Controlled Release*, 2018, **286**, 301–314, DOI: **10.1016/j.jconrel.2018.08.001**.

44 S. M. Lewis, A. Williams and S. C. Eisenbarth, Structure and Function of the Immune System in the Spleen, *Sci. Immunol.*, 2019, **4**(33), eaau6085, DOI: **10.1126/sciimmunol.aau6085**.

45 K. A. E. Sayed, M. A. Khanfar, H. M. Shallal, A. Muralidharan, B. Awate, D. T. A. Youssef, Y. Liu, Y.-D. Zhou, D. G. Nagle and G. Shah, Latrunculin A and Its C-17-*O*-Carbamates Inhibit Prostate Tumor Cell Invasion and HIF-1 Activation in Breast Tumor Cells, *J. Nat. Prod.*, 2008, **71**(3), 396–402, DOI: **10.1021/np070587w**.

46 L. Shojaie, A. Iorga and L. Dara, Cell Death in Liver Diseases: A Review, *Int. J. Mol. Sci.*, 2020, **21**(24), 9682, DOI: **10.3390/ijms21249682**.

47 M. P. Vincent, T. Stack, A. Vahabikashi, G. Li, K. M. Perkumas, R. Ren, H. Gong, W. D. Stamer, M. Johnson and E. A. Scott, Surface Engineering of FLT4-Targeted Nanocarriers Enhances Cell-Softening Glaucoma Therapy, *ACS Appl. Mater. Interfaces*, 2021, **13**(28), 32823–32836, DOI: **10.1021/acsami.1c09294**.

48 S. A. Yuk, H. Kim, N. S. Abutaleb, A. M. Dieterly, M. S. Taha, M. D. Tsifansky, L. T. Lyle, M. N. Seleem and Y. Yeo, Nanocapsules Modify Membrane Interaction of Polymyxin B to Enable Safe Systemic Therapy of Gram-negative Sepsis, *Sci. Adv.*, 2021, **7**(32), eabj1577, DOI: **10.1126/sciadv.abj1577**.

49 M. Siwicki, N. A. Gort-Freitas, M. Messemaker, R. Bill, J. Gungabeesoon, C. Engblom, R. Zilionis, C. Garris, G. M. Gerhard, A. Kohl, Y. Lin, A. E. Zou, C. Cianciaruso, E. Bolli, C. Pfirschke, Y.-J. Lin, C. Piot, J. E. Mindur, N. Talele, R. H. Kohler, Y. Iwamoto, M. Mino-Kenudson, S. I. Pai, C. deVito, T. Koessler, D. Merkler, A. Coukos, A. Wicky, M. Fraga, C. Sempoux, R. K. Jain, P.-Y. Dietrich, O. Michielin, R. Weissleder, A. M. Klein and M. J. Pittet, Resident Kupffer Cells and Neutrophils Drive Liver Toxicity in Cancer Immunotherapy, *Sci. Immunol.*, 2021, **6**(61), eabi7083, DOI: **10.1126/sciimmunol.abi7083**.

50 N. Van Rooijen and E. Van Kesteren-Hendrikx, Clodronate Liposomes: Perspectives In Research And Therapeutics, *J. Liposome Res.*, 2002, **12**(1–2), 81–94, DOI: **10.1081/LPR-120004780**.

51 F. Jönsson, C. B. Gurniak, B. Fleischer, G. Kirfel and W. Witke, Immunological Responses and Actin Dynamics in Macrophages Are Controlled by N-Cofilin but Are Independent from ADF, *PLoS One*, 2012, **7**(4), e36034, DOI: **10.1371/journal.pone.0036034**.

52 B. Simonetti and P. J. Cullen, Actin-Dependent Endosomal Receptor Recycling, *Curr. Opin. Cell Biol.*, 2019, **56**, 22–33, DOI: **10.1016/j.ceb.2018.08.006**.

53 J. Cendrowski, A. Mamińska and M. Miaczynska, Endocytic Regulation of Cytokine Receptor Signaling, *Cytokine Growth Factor Rev.*, 2016, **32**, 63–73.

54 W.-W. Lin, Y.-C. Lu, C.-H. Chuang and T.-L. Cheng, Ab Locks for Improving the Selectivity and Safety of Antibody Drugs, *J. Biomed. Sci.*, 2020, **27**(1), 76, DOI: **10.1186/s12929-020-00652-z**.

55 L.-X. Wang, X. Tong, C. Li, J. P. Giddens and T. Li, Glycoengineering of Antibodies for Modulating Functions, *Annu. Rev. Biochem.*, 2019, **88**, 433–459, DOI: **10.1146/annurev-biochem-062917-012911**.

56 E. L. Korn, J. A. Moscow and B. Freidlin, Dose Optimization during Drug Development: Whether and When to Optimize, *J. Natl. Cancer Inst.*, 2023, **115**(5), 492–497, DOI: **10.1093/jnci/djac232**.

57 S. Yi, S.-Y. Kim, M. P. Vincent, S. A. Yuk, S. Bobbala, F. Du and E. A. Scott, Dendritic Peptide-Conjugated Polymeric Nanovectors for Non-Toxic Delivery of Plasmid DNA and Enhanced Non-Viral Transfection of Immune Cells, *iScience*, 2022, **25**(7), 104555, DOI: **10.1016/j.isci.2022.104555**.

